



The Shigella type III effector IpgD recodes Ca²⁺ signals during invasion of epithelial cells

Chun Hui Sun, Benjamin Wacquier, Daniel Aguilar, Nathalie Carayol, Kevin Denis, Sylviane Boucherie, Cesar Valencia-Gallardo, Ceren Simsek, Christophe Erneux, Alexandre Lehman, et al.

► To cite this version:

Chun Hui Sun, Benjamin Wacquier, Daniel Aguilar, Nathalie Carayol, Kevin Denis, et al.. The Shigella type III effector IpgD recodes Ca²⁺ signals during invasion of epithelial cells. EMBO Journal, 2017, 36 (17), pp.2567 - 2580. 10.15252/emboj.201696272 . pasteur-01899400

HAL Id: pasteur-01899400

<https://pasteur.hal.science/pasteur-01899400>

Submitted on 19 Oct 2018

HAL is a multi-disciplinary open access archive for the deposit and dissemination of scientific research documents, whether they are published or not. The documents may come from teaching and research institutions in France or abroad, or from public or private research centers.

L'archive ouverte pluridisciplinaire **HAL**, est destinée au dépôt et à la diffusion de documents scientifiques de niveau recherche, publiés ou non, émanant des établissements d'enseignement et de recherche français ou étrangers, des laboratoires publics ou privés.

Copyright

SOURCE
DATATRANSPARENT
PROCESS

The *Shigella* type III effector IpgD recodes Ca^{2+} signals during invasion of epithelial cells

Chun Hui Sun^{1,2,3,4,5,6}, Benjamin Wacquier⁷, Daniel I Aguilar^{1,2,3,4}, Nathalie Carayol^{1,2,3,4}, Kevin Denis^{1,2,3,4} , Sylviane Boucherie^{5,6}, Cesar Valencia-Gallardo^{1,2,3,4}, Ceren Simsek^{1,2,3,4}, Christophe Erneux⁸, Alexandre Lehman⁸, Jost Enninga⁹, Laurence Arbibe¹⁰, Philippe Sansonetti^{11,12,13}, Geneviève Dupont⁷, Laurent Combettes^{5,6,†} & Guy Tran Van Nhieu^{1,2,3,4,*†}

Abstract

The role of second messengers in the diversion of cellular processes by pathogens remains poorly studied despite their importance. Among these, Ca^{2+} virtually regulates all known cell processes, including cytoskeletal reorganization, inflammation, or cell death pathways. Under physiological conditions, cytosolic Ca^{2+} increases are transient and oscillatory, defining the so-called Ca^{2+} code that links cell responses to specific Ca^{2+} oscillatory patterns. During cell invasion, *Shigella* induces atypical local and global Ca^{2+} signals. Here, we show that by hydrolyzing phosphatidylinositol-(4,5)bisphosphate, the *Shigella* type III effector IpgD dampens inositol-(1,4,5)trisphosphate (InsP_3) levels. By modifying InsP_3 dynamics and diffusion, IpgD favors the elicitation of long-lasting local Ca^{2+} signals at *Shigella* invasion sites and converts *Shigella*-induced global oscillatory responses into erratic responses with atypical dynamics and amplitude. Furthermore, IpgD eventually inhibits InsP_3 -dependent responses during prolonged infection kinetics. IpgD thus acts as a pathogen regulator of the Ca^{2+} code implicated in a versatility of cell functions. Consistent with this function, IpgD prevents the Ca^{2+} -dependent activation of calpain, thereby preserving the integrity of cell adhesion structures during the early stages of infection.

Keywords calcium; calpain; IpgD; *Shigella*; talin

Subject Categories Microbiology, Virology & Host Pathogen Interaction; Signal Transduction

DOI 10.15252/embj.201696272 | Received 7 December 2016 | Revised 3 June 2017 | Accepted 13 June 2017 | Published online 12 July 2017

The EMBO Journal (2017) 36: 2567–2580

Introduction

To efficiently colonize tissue and promote infection, pathogens divert host cell signals to induce cytoskeletal rearrangements, or regulate inflammatory signals and tissue integrity (Ashida *et al*, 2012; Valdivia & Sedwick, 2014; LaRock *et al*, 2015). In most infection models, however, the role of second messengers has been poorly studied despite their being critical for fundamental functions. Among these, Ca^{2+} has been involved in the regulation of virtually all known cell processes, including cytoskeletal reorganization, inflammation, or cell death pathways (Berridge *et al*, 2000; Murakami *et al*, 2012; Rizzuto *et al*, 2012). Under physiological conditions, cytosolic Ca^{2+} increases are transient and often oscillatory, being regulated by an interplay between pumps and channels at the endoplasmic reticulum and plasma membranes (Berridge *et al*, 2000; Strehler, 2015). The discovery of a so-called Ca^{2+} code, associating different cell responses with specific Ca^{2+} oscillatory patterns, has brought up mechanistic insights into Ca^{2+} signaling and has established modeling as unique means to apprehend the complexity of Ca^{2+} processes in integrated systems (Muallem, 2005; Uhlen & Fritz, 2010). *Shigella*, the agent of bacillary dysentery, invades colonic epithelial cells where it disseminates causing an intense inflammation responsible for the destruction of the mucosa

1 Equipe Communication InterCellulaire et Infections Microbiennes, Centre de Recherche Interdisciplinaire en Biologie (CIRB), Collège de France, Paris, France

2 Institut National de la Santé et de la Recherche Médicale (INSERM) U1050, Paris, France

3 Centre National de la Recherche Scientifique (CNRS) UMR7241, Paris, France

4 MEMOLIFE Laboratory of excellence and Paris Sciences et Lettres, Paris, France

5 Université Paris Sud, Orsay, France

6 Inserm, UMR51174, Orsay, France

7 Unité de Chronobiologie Théorique, Université Libre de Bruxelles, Brussels, Belgium

8 Interdisciplinary Research Institute (IRIBHM), Université Libre de Bruxelles, Brussels, Belgium

9 Département de Biologie Cellulaire et Infection, Institut Pasteur, Unité de la Dynamique des Interactions Hôte-Pathogène, Paris, France

10 Equipe Plasticité du Génome et Infection, INSERM UMR_S1151 – CNRS UMR8253, Institut Necker Enfants Malades (INEM), Université Paris Descartes, Paris, France

11 Département de Biologie Cellulaire et Infection, Unité de Pathogénie Microbienne Moléculaire, Paris, France

12 Unité Inserm 1202, Institut Pasteur, Paris, France

13 Collège de France, Paris, France

*Corresponding author. Tel: +33 1 44271489; E-mail: guy.tran-van-nhieu@college-de-france.fr

†These authors contributed equally to this work

(Ashida *et al*, 2012; Tanner *et al*, 2015). Disease progression involves an arsenal of bacterial effectors enabling lysis of the phagocytic vacuole, intracellular replication, and bacterial spreading (Kuehl *et al*, 2015). *Shigella* effectors injected in the host cell cytosol by the *Shigella* type III secretion system (T3SS) play a major role in these different steps (Galan *et al*, 2014; Ashida *et al*, 2015). While *Shigella* intracellular replication eventually leads to epithelial cell destruction, efficient bacterial spreading requires the delay of cell death processes and the maintenance of cell integrity (Carneiro *et al*, 2009; Ashida *et al*, 2014). During invasion, *Shigella* triggers InsP_3 -dependent Ca^{2+} responses that differ from agonist-induced Ca^{2+} responses. *Shigella*-induced Ca^{2+} responses consist of isolated global increases of varying amplitude and dynamics, as well as local Ca^{2+} responses with durations exceeding several seconds termed RATPs for responses associated with trespassing pathogens (Tran Van Nhieu *et al*, 2013). We reasoned that the atypical aspects of these responses were due to the action of one or several bacterial effectors. Among *Shigella* effectors, the type III effector IpgD is as a phosphatidyl-(4, 5)bisphosphate ($\text{PI}(4,5)\text{P}_2$)-4-phosphatase regulating cytoskeletal remodeling, cell survival, endosomal trafficking, or macropinosome formation around invading bacteria (Niebuhr *et al*, 2002; Konradt *et al*, 2011; Mellouk *et al*, 2014; Boal *et al*, 2016; Weiner *et al*, 2016). $\text{PI}(4,5)\text{P}_2$ is the main substrate used by phospholipases C (PLCs) to produce InsP_3 , and it is expected that a general depletion of $\text{PI}(4,5)\text{P}_2$ will impact on InsP_3 levels. However, as opposed to agonists acting diffusely and synchronously on cell surface receptors triggering InsP_3 -mediated Ca^{2+} release, *Shigella* only interacts with a discrete area of the cell plasma membrane and invasion events are not synchronized. As a consequence, the overall levels of cell substrates targeted by injected type III effectors are not expected to be limiting, in particular at the onset of the invasion process. It is therefore unclear whether the $\text{PI}(4,5)\text{P}_2$ phosphatase activity of IpgD could affect Ca^{2+} signaling during bacterial invasion. Any detected effects could provide insights into the local aspect of bacterial stimulation and the transition from local to global Ca^{2+} responses. These reasons prompted us to study the effects of IpgD on Ca^{2+} signaling during bacterial invasion.

Results

IpgD down-regulates the recruitment of InsP_3 receptors and InsP_3 levels during *Shigella* invasion

During *Shigella* invasion, the atypical duration of bacterial-induced local Ca^{2+} responses was shown to depend on the confinement of InsP_3 and enrichment of InsP_3 receptors (IP3Rs) at bacterial entry sites (Tran Van Nhieu *et al*, 2013). We reasoned that through its action on $\text{PI}(4,5)\text{P}_2$, IpgD could regulate InsP_3 -mediated signaling.

We first analyzed the effects of IpgD on the recruitment of the InsP_3 receptors at invasion foci induced by an *ipgD* mutant isogenic to wild-type *Shigella* (Niebuhr *et al*, 2002). As shown in Fig 1A and B and as previously observed in HeLa cells, the InsP_3 receptor type 1 (IP3R1) was enriched by 1.5-fold as early as 5 min following bacterial challenge for both wild-type and *ipgD* mutant strains. While this enrichment factor only moderately increased for wild-type *Shigella* at later stages of focus formation, however, invasion foci induced by the *ipgD* mutant showed a drastic increase in IP3R1

enrichment, reaching 2.2-fold after 30 min (Fig 1B). Consistent with a role for IpgD-mediated hydrolysis of $\text{PI}(4,5)\text{P}_2$ in IP3R1 recruitment, invasion foci induced by an *ipgD* mutant complemented with catalytically inactive IpgD C438S also showed a similar increase in IP3R1 enrichment compared to the *ipgD* strain complemented with wild-type IpgD (Fig EV1).

We next wanted to determine whether IpgD affected the levels of InsP_3 during *Shigella* invasion. Cells were metabolically labeled with H^3 -inositol, and inositol-polyphosphates (InsPPs) were measured (Materials and Methods). As shown in Fig 1C, among the InsPPs , InsP_3 levels were much higher in cells infected with the *ipgD* mutant as compared to WT *Shigella*. For both strains, however, InsP_3 dropped to undetectable levels after 150 min of infection, suggesting that IpgD regulated InsP_3 -mediated signaling during the early phases of infection (Fig 1D). Together, these results are consistent with the depletion of $\text{PI}(4,5)\text{P}_2$ by IpgD, leading to decreased InsP_3 levels during *Shigella* invasion. When $\text{PI}(4,5)\text{P}_2$ recruitment was analyzed at *Shigella* invasion sites with a GFP-PH-PLC δ probe (Materials and Methods; Balla & Varnai, 2009), enrichment could be detected as early as 5 min following cell contact and peaked at 15 min, with kinetics that paralleled those of bacterial internalization (Appendix Fig S1). Similar to IP3R1, $\text{PI}(4,5)\text{P}_2$ recruitment at foci induced by the *ipgD* mutant was significantly higher than that observed in foci induced by WT *Shigella* (Appendix Fig S1).

To confirm these results in a more relevant cell system, we analyzed the recruitment of IP3R in intestinal epithelial TC7 cell monolayers that were allowed to polarize for 7 days (Materials and Methods). As opposed to HeLa cells, TC7 cells do not express IP3R1 but mainly IP3R type 3 (IP3R3) (Shibao *et al*, 2010). Apical staining of the junctional marker ZO-1 confirmed that cells were polarized under the conditions used (Appendix Fig S2A). As shown in Fig 1E, polarized TC-7 cells presented a granular pattern of IP3R3 diffusely distributed over their cytoplasm. As previously observed, while much less efficient than in non-polarized HeLa cells, bacterial invasion could also be detected at the apical surface of polarized TC7 cells (Mounier *et al*, 1992; Romero *et al*, 2011). IP3R3 recruitment could be detected at these invasion sites, with IP3R3 trapped within or outlining bacterial-induced actin foci (Figs 1E and EV3B). As observed for IP3R1 in non-polarized cells, recruitment was more important in foci induced by the *ipgD* mutant compared to wild-type *Shigella* (Fig 1E and F, Appendix Fig S2B).

Together, these results indicate that IpgD down-regulates the recruitment of IP3Rs and InsP_3 levels during *Shigella* invasion.

IpgD shapes Ca^{2+} responses during *Shigella* invasion

Shigella induces sustained atypical local Ca^{2+} responses that are associated with bacterial invasion (Tran Van Nhieu *et al*, 2013). Since these responses depend on InsP_3 -mediated Ca^{2+} signaling, we investigated the role of IpgD in Ca^{2+} signals during *Shigella* invasion. For this, cells were loaded with the Ca^{2+} fluorescent indicator Fluo-4, challenged with bacteria, and subjected to high-speed fluorescent microscopy analysis to detect local Ca^{2+} transients.

As shown in Fig 2A and as observed previously, local Ca^{2+} responses with atypically long duration (RATPs) and associated with bacterial invasion sites could be detected in cells infected with the *Shigella* wild-type strain (Fig 2A, WT). Upon cell invasion, the *ipgD* mutant elicited local responses at a similar

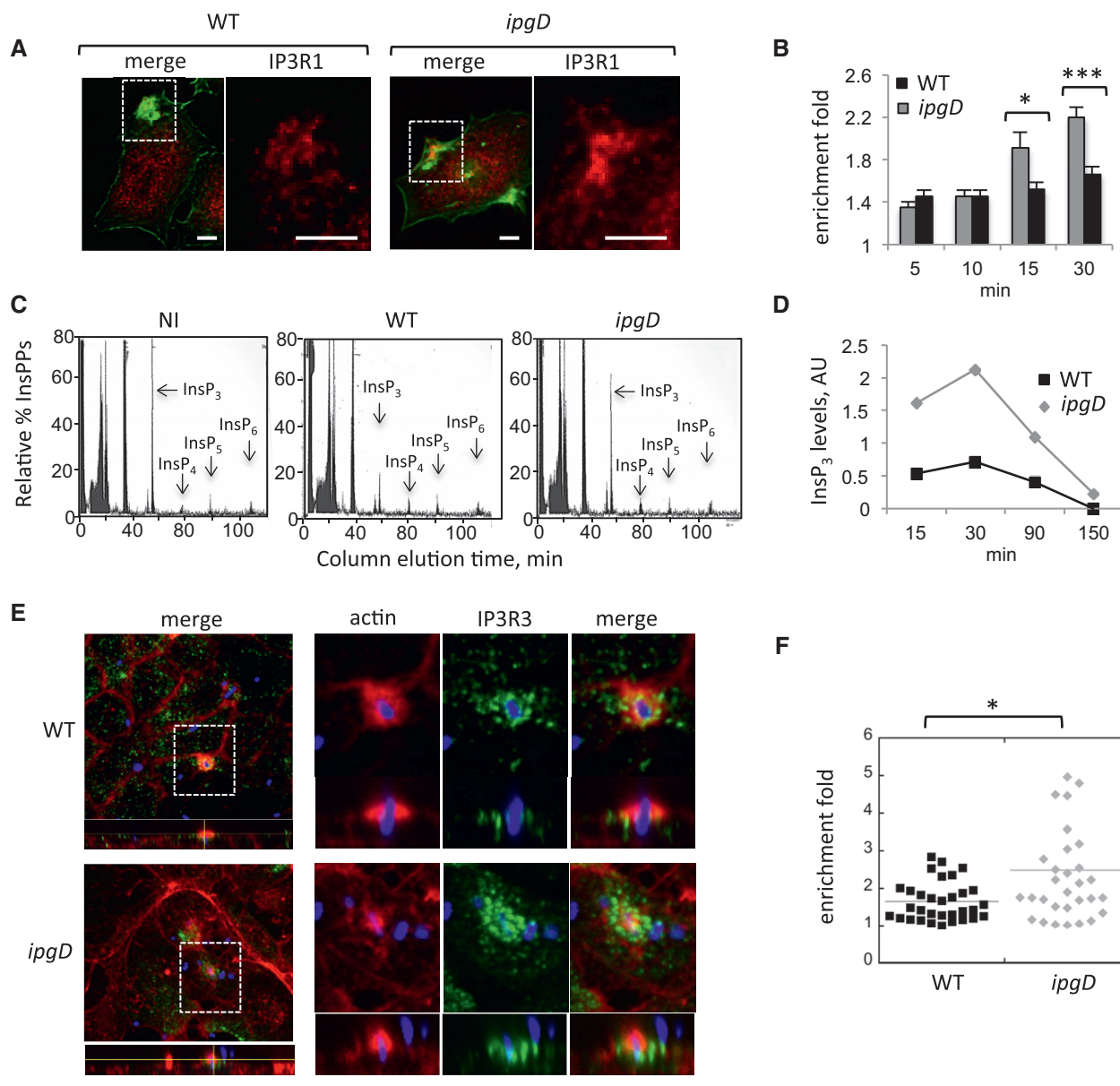


Figure 1. IpgD down-regulates IP3R recruitment and InsP_3 levels during *Shigella* invasion.

- A Representative confocal fluorescence images of cells challenged with the indicated bacterial strains for 15 min at 37°C and processed for immunofluorescence staining. The right panels are higher magnifications of the corresponding boxed inset. Red: IP3R1; green: actin. Scale bar = 5 μm .
- B The enrichment fold of IP3R1 at invasion foci \pm SEM was determined at the indicated time points (Materials and Methods). WT *Shigella*: solid bars; *ipgD* mutant: gray bars. $N = 3,200$ foci. Wilcoxon test, * $P = 0.0220$; *** $P = 2.7 \times 10^{-15}$.
- C Cells were labeled with H^3 -myo-inositol and challenged with the indicated bacteria for 30 min at 37°C. IPPs were analyzed by anion-exchange chromatography as described (Leyman et al, 2007). InsP elution profiles are shown. Note the decrease in InsP_3 levels during infection with WT *Shigella*.
- D The ratio of InsP_3 relative to initial levels in uninfected cells was determined from measurements as in panel (C) in extracts from cells challenged with WT *Shigella* (black squares) or the *ipgD* mutant (gray diamonds). The time post-infection is indicated.
- E Polarized TC7 cell monolayers were challenged with the indicated bacterial strains for 20 min at 37°C and processed for immunofluorescence staining. The IP3R3 panel is a higher magnification of the corresponding boxed inset. Green: IP3R3; red: actin; blue: bacterial LPS. Scale bar = 5 μm .
- F The enrichment fold of IP3R3 at invasion foci was determined for the indicated strains. Each mark represents a determination. $N = 2$, Wilcoxon test, * $P = 0.033$.

frequency, but significantly less RATPs than WT *Shigella* (Fig 2B). Instead, the *ipgD* mutant induced fast spiking and oscillating local Ca^{2+} responses reminiscent of repetitive puffs that were seldom observed with WT *Shigella* (Fig 2A, middle panels). Strikingly, the *ipgD* mutant elicited more global Ca^{2+} responses than WT

Shigella, with 40.3 ± 7.5 (SEM) % and 11.3 ± 4.4 (SEM) % of cells showing global responses in the case of the *ipgD* mutant and WT after 15 min, respectively (Fig 2B). Consistent with InsP_3 -mediated Ca^{2+} release, cell treatment with the PLC inhibitor U73122 virtually abolished local and global Ca^{2+} responses

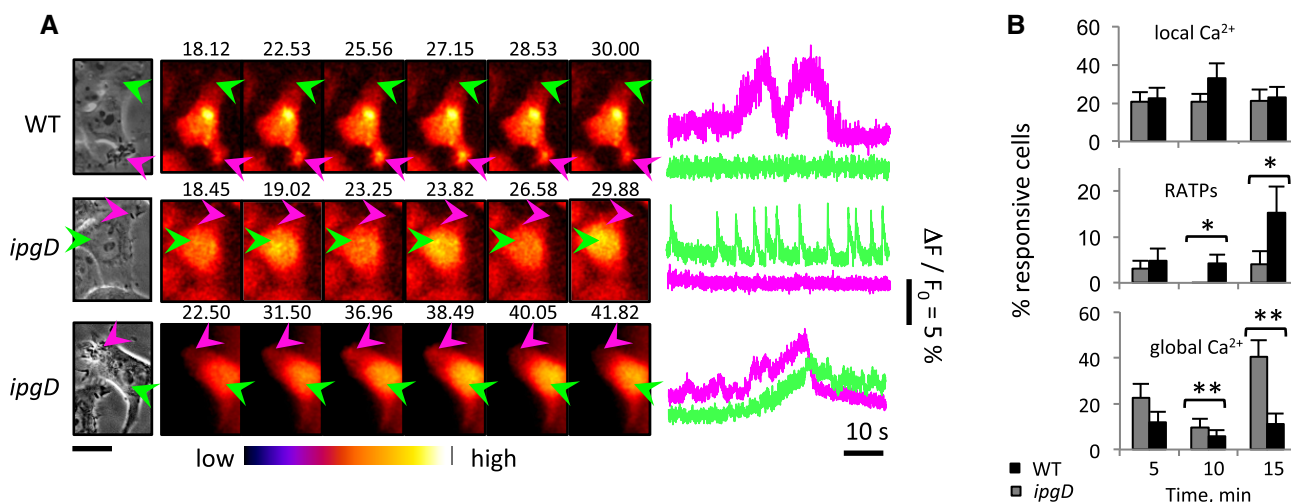


Figure 2. IpgD shapes local and global Ca^{2+} responses during *Shigella* invasion.

A HeLa cells were loaded with Fluo-4-AM and challenged with the indicated bacterial strains. Left: Phase-contrast images. Center: Time series of Fluo-4 fluorescence of the corresponding fields depicted with the indicated color code. The elapsed time from the start of acquisition is indicated in seconds. Arrowheads: invasion foci (purple); control area (green). Scale bar = 5 μm . Right: Traces of Ca^{2+} variations in area pointed to by the arrow with the corresponding color in left panels. From top to bottom, these traces are representative of local RATPs, local fast spiking, and global responses.

B Percentage of cells \pm SEM showing local responses, RATPs, or global Ca^{2+} responses induced by the *ipgD* mutant (gray bars) or WT *Shigella* (black bars). $N = 4$, > 60 cells for each determination. Wilcoxon test, * $P < 0.05$; ** $P < 0.01$.

induced by wild-type *Shigella* and the *ipgD* mutant (Fig EV2). Catalytically inactive IpgD C438S did not complement the *ipgD* mutant, indicating that the IpgD phosphatase activity was required for the confinement of Ca^{2+} responses at invasion sites (Fig EV3). Of note, because of the higher MOI required to perform Ca^{2+} imaging with these complemented strains, higher percentages of Ca^{2+} -responsive cells were observed during bacterial challenge at 5 min post-infection (Fig EV3). At these early time points of infection, however, the *ipgD*/IpgD C438S strain induced more responses than the *ipgD*/IpgD complemented strain, consistent with the catalytic activity of IpgD in the down-regulation and confinement of Ca^{2+} responses at invasion sites.

These results indicated that IpgD, through its $\text{PI}(4,5)\text{P}_2$ phosphatase activity, is involved in the confinement of Ca^{2+} responses at *Shigella* invasion sites. In the absence of IpgD, *Shigella* triggered less local and more global Ca^{2+} transients during cell invasion.

Invasion foci induced by the *ipgD* mutant are less restrictive in diffusion than WT foci

In addition to its effects on InsP_3 production, IpgD has been reported to favor the polymerization of actin at *Shigella* entry sites by disconnecting cortical actin from the plasma membrane or alternatively, through $\text{PI}(5)\text{P}$ synthesis and activation of Tiam-1, a guanine exchange factor (GEF) for the Cdc42 and Rac GTPases (Niebuhr *et al*, 2002). We also reported that InsP_3 -mediated signaling contributes to actin polymerization at *Shigella* invasion sites (Tran Van Nhieu *et al*, 2013), suggesting that through the regulation of InsP_3 levels and confinement of Ca^{2+} signals reported in this study, IpgD may also affect actin dynamics. Since actin polymerization may in turn restrict diffusion, IpgD could therefore control Ca^{2+} signals by dampening InsP_3 synthesis at its point source, as well as its diffusion at invasion sites.

We thus wanted to clarify whether differences in actin polymerization sites could affect the diffusion parameters in foci induced by the *ipgD* mutant compared to wild-type *Shigella*.

Consistent with the reported effects of IpgD on actin polymerization (Niebuhr *et al*, 2002), actin foci induced by the *ipgD* mutant were smaller in size and were less dense compared to foci induced by WT (Fig 3A–C). In previous works, the restriction of diffusion due to actin polymerization at entry sites was shown to determine the atypical long-lasting local Ca^{2+} responses during *Shigella* invasion (Tran Van Nhieu *et al*, 2013). To test the diffusion properties in actin foci induced by the *ipgD* mutant, we performed fluorescence recovery after photobleaching (FRAP) experiments on cells loaded with the freely diffusible fluorescent dye calcein and infected with bacteria (Materials and Methods). As shown in Fig 3D and E and as previously observed, actin foci induced by WT *Shigella* showed calcein fluorescence recovery kinetics that were consistent with restricted diffusion, with a half-maximal recovery time ($T_{1/2}$) of 347 ± 25 (SEM) ms, compared to 222 ± 14 (SEM) ms for free diffusion in control area (Tran Van Nhieu *et al*, 2013). Consistent with the lesser density of polymerized actin in foci induced by the *ipgD* mutant, however, the determined average $T_{1/2}$ corresponded to 287 ± 22 (SEM) ms, which indicates that diffusion was not as restricted as that observed in WT-induced foci.

Thus, foci induced by the *ipgD* mutant show a restriction of diffusion, which, while less pronounced than that observed for wild-type *Shigella*, may restrict the extent of InsP_3 propagation and impact on bacterial-induced Ca^{2+} signals.

Modeling points to a critical role for IpgD in regulating *Shigella*-induced local and global Ca^{2+} responses

Using computational modeling, we previously showed that restricted diffusion and increased InsP_3 synthesis at invasion sites

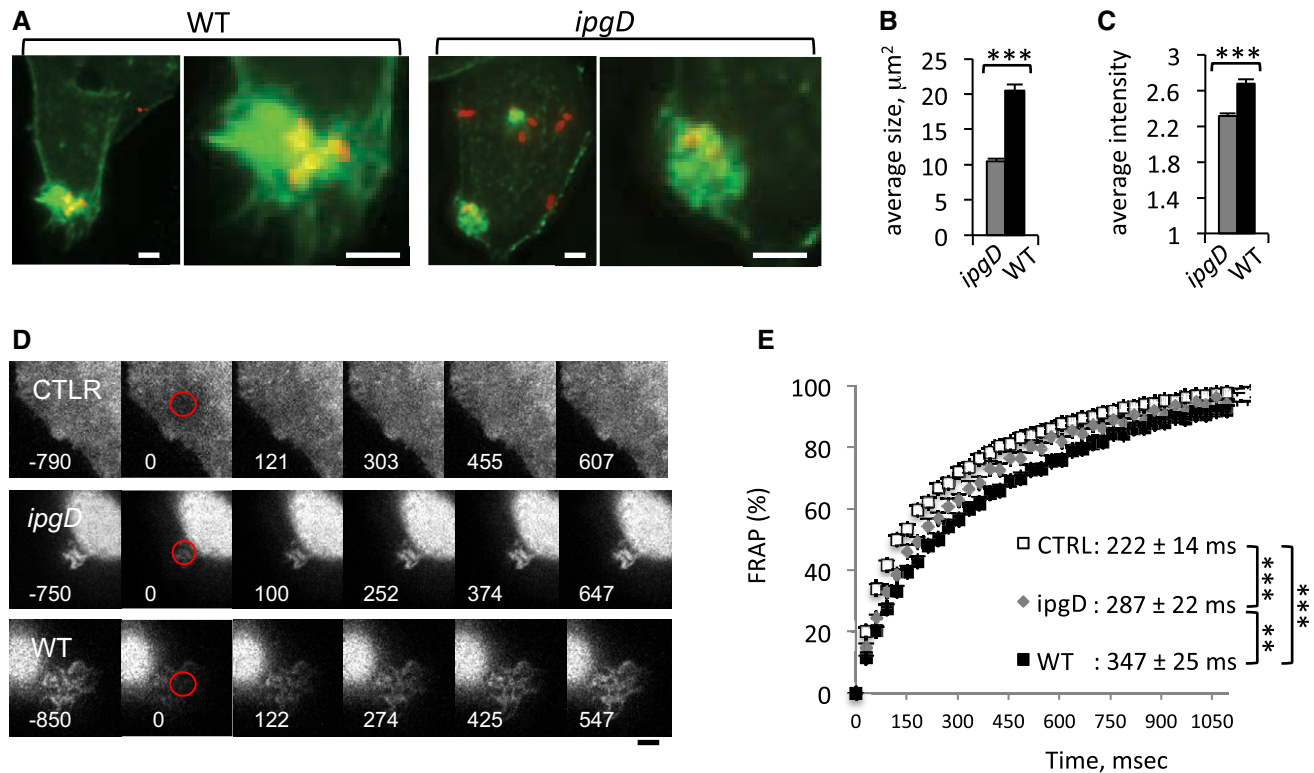


Figure 3. Invasion foci induced by the *ipgD* mutant are less restrictive in diffusion than foci induced by WT *Shigella*.

- A** Representative fluorescent confocal micrographs of cells challenged with the indicated bacterial strains for 15 min at 37°C and processed for fluorescence staining of F-actin (green) and bacteria (red). Right: Larger magnification of the insets depicted in the left panels. Scale bar, 5 μm .
- B** The average size of invasion foci stained with fluorescent phalloidin \pm SEM is indicated for each bacterial strain ($N = 3$; $n > 35$). Wilcoxon test, $***P < 0.001$.
- C** The relative fluorescence intensity of invasion foci stained with fluorescent phalloidin \pm SEM is indicated for each bacterial strain ($N = 3$; $n > 35$). Unpaired *t*-test, $***P < 0.001$.
- D** Representative time-lapse images of cells loaded with calcein, challenged with the indicated bacteria, and subjected to FRAP analysis. Red: bleached area. The time after bleach is indicated in ms. Scale bar = 5 μm .
- E** Fluorescence recovery kinetics in % in control area (empty squares), foci induced by wild-type *Shigella* (solid squares) or *ipgD* mutant (gray diamonds). The traces represent the average of more than 27 determinations in three independent experiments. The estimated half-maximal recovery times ($T_{1/2}$) \pm SEM are indicated. Unpaired *t*-test, WT vs. *ipgD*: $**P = 0.0076$; WT vs control or *ipgD* vs control: $***P < 0.0001$.

accounted for local and long-lasting Ca^{2+} responses (RATPs) observed during invasion of WT *Shigella* (Tran Van Nhieu *et al*, 2013). We then used the model to investigate the respective roles of restricted diffusion and InsP_3 levels in IpgD-mediated confinement of Ca^{2+} responses during *Shigella* invasion (Materials and Methods). Typical local RATPs and global Ca^{2+} responses obtained by simulation of the model are shown in Fig 4A and B. In agreement with experimental observations, when scoring responding cells, the *ipgD* mutant showed more global and less local Ca^{2+} responses than WT *Shigella*, with 80% of global and 20% of local responses for the *ipgD* mutant, and 60% of global and 40% of local responses for WT *Shigella* (Fig 4C). According to the model, the diffusivity characteristics and the rate of InsP_3 synthesis determined for the *ipgD* mutant were both important in defining the local versus global character of the Ca^{2+} response. By decreasing the rate of InsP_3 synthesis, IpgD limited the propagation of this messenger in the bulk of the cytoplasm. Indeed, if only taking into account an increased rate of InsP_3 synthesis, the proportion of global responses increased to 68% (Fig 4C, middle panel). The higher diffusivity accounted for the higher percentage (80%) of global responses in the *ipgD* mutant.

When modeled during prolonged kinetics of bacterial infection, the rates of InsP_3 synthesis at invasion sites were larger for the *ipgD* mutant, with $J_{\text{IP}} = 4.5 \mu\text{M/s}$ compared to $2.5 \mu\text{M/s}$ for WT, in agreement with the experimental determinations of levels of InsP_3 in Fig 1. The model reproduced the occurrence of irregular and small-amplitude Ca^{2+} increases during infection by WT *Shigella* and predicted regular and spiky Ca^{2+} oscillations for the *ipgD* mutant (Fig 4D). The shift in the pattern of Ca^{2+} dynamics observed in the *ipgD* mutant was due to larger InsP_3 concentrations, favoring high-amplitude and regular Ca^{2+} responses (Dupont *et al*, 2008; Thurley *et al*, 2014).

IpgD inhibits Ca^{2+} signals during prolonged infection kinetics

When experimentally investigated, WT *Shigella* induced atypical isolated Ca^{2+} responses during the first 30 min of infection, but a drastic decrease in amplitude and frequency of these responses was observed during further incubation (Fig 5A). In contrast and consistent with the model, cells infected with the *ipgD* mutant showed responses with sharp increases and oscillations reminiscent of Ca^{2+}

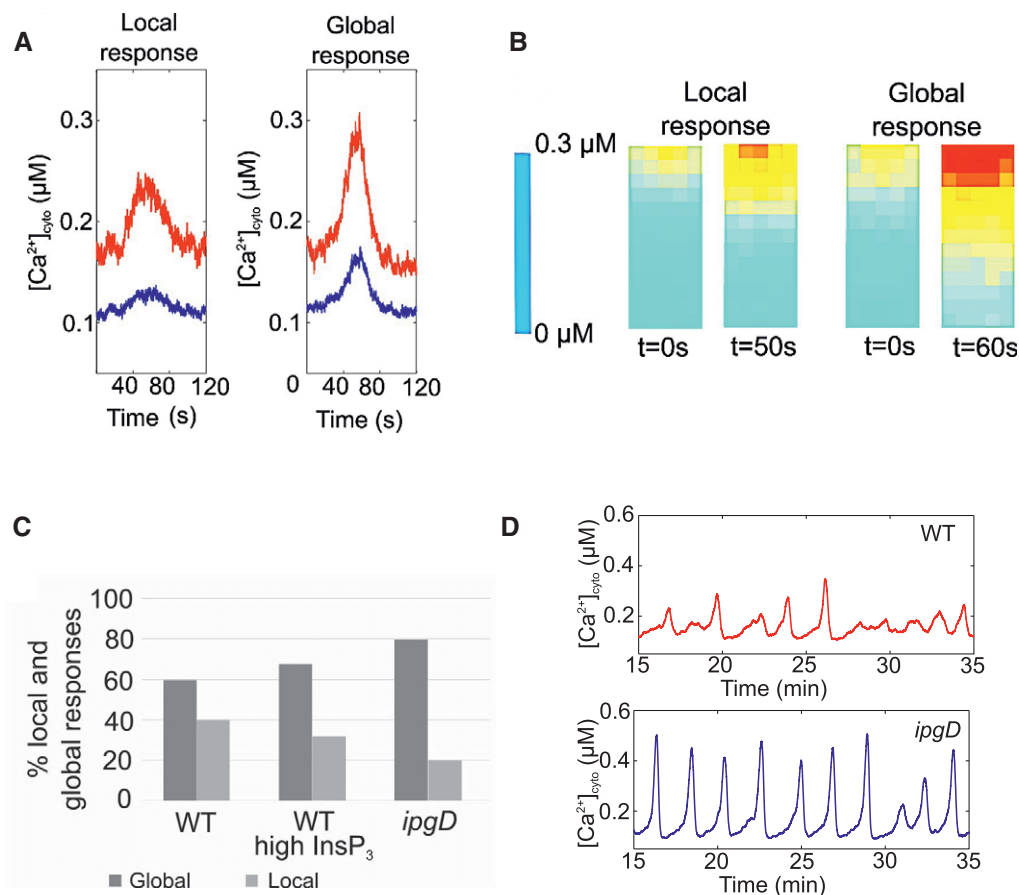


Figure 4. Modeling the effects of IpgD on *Shigella*-induced Ca^{2+} responses.

- A Representative local and global Ca^{2+} responses obtained by stochastic simulations of the model defined by equations 1–3 (Table EV1). Variations of Ca^{2+} concentrations at the invasion site (red) and in the middle of the cell (blue).
- B Spatial profiles of Ca^{2+} concentrations corresponding to simulations shown in panel (A). The geometry of the system is depicted in Appendix Fig S7.
- C Percentages of local (gray bars) and global (solid bars) Ca^{2+} responses in cells challenged with WT *Shigella*, WT with InsP_3 levels estimated for the *ipgD* mutant (WT with high InsP_3), and *ipgD* mutant.
- D Prediction of Ca^{2+} responses induced by WT *Shigella* or by the *ipgD* mutant over prolonged infection kinetics. Parameter values are those listed in Table EV1, except for $j_{\text{IP}} = 2.5 \mu\text{M/s}$ and $4.5 \mu\text{M/s}$ for the WT and the *ipgD* mutant, respectively.

responses to agonists, which were still elicited after 30 min of bacterial infection (Fig 5A). After bacterial incubation for 90 min, cells infected with WT *Shigella* showed a clear inhibition in the elicitation of Ca^{2+} responses to agonist compared to cells infected with the *ipgD* mutant (Fig 5B), with 40.4 ± 1.6 (SEM) % compared to 59.1 ± 7.4 (SEM) % of cells responding to $0.5 \mu\text{M}$ histamine, respectively ($N = 3$, $n > 45$ cells). Furthermore, at this histamine concentration, WT *Shigella*-infected cells showed Ca^{2+} responses with an average amplitude of 13.9 ± 3.8 (SEM) % of the maximal response, compared to 46 ± 8.4 (SEM) % for cells infected with the *ipgD* mutant ($N = 3$, $n > 45$ cells; Fig 5C). As expected, the *ipgD* complemented with catalytically active IpgD was less responsive to histamine stimulation than the *ipgD*/IpgD C438S strain (Fig EV3F).

To determine whether IpgD was sufficient to account for the inhibition of Ca^{2+} signaling, cells were transfected with a GFP-IpgD construct, and their ability to respond to agonists stimulating InsP_3 -dependent Ca^{2+} responses was analyzed. As shown in Fig EV4, GFP-IpgD-transfected cells were unresponsive to $0.2 \mu\text{M}$ histamine or $1 \mu\text{M}$ ATP, as opposed to cells transfected with catalytically

inactive GFP-IpgDC438S. Furthermore, GFP-IpgD transfectants showed more than a fivefold decrease in the percentage of responding cells when stimulated at $2 \mu\text{M}$ histamine or $5 \mu\text{M}$ ATP compared to control cells (Fig EV4).

When analyzed during *Shigella* invasion of polarized TC7 cells, Ca^{2+} responses were reminiscent of those observed in HeLa cells, with isolated responses of various amplitudes. However, pseudo-oscillatory responses were not detected even upon challenge with the *ipgD* mutant strain (Fig 5D). These results are in line with a poorer efficiency of *Shigella* invasion in these cells compared to non-polarized cells (Mounier *et al*, 1992; Romero *et al*, 2011). Strikingly, however, as opposed to cells challenged with the *ipgD* mutant, cells challenged with wild-type *Shigella* showed a sharp decrease in the occurrence of Ca^{2+} responses during the incubation period, with very few responses elicited after 30 min of bacterial challenge (Fig 5D). When quantified during this period, the percentage of cells showing responses was significantly different between these samples, with 42 ± 6 compared to 78 ± 7 (SEM) % of responsive cells for challenge with wild-type *Shigella* and the *ipgD* mutant, respectively.

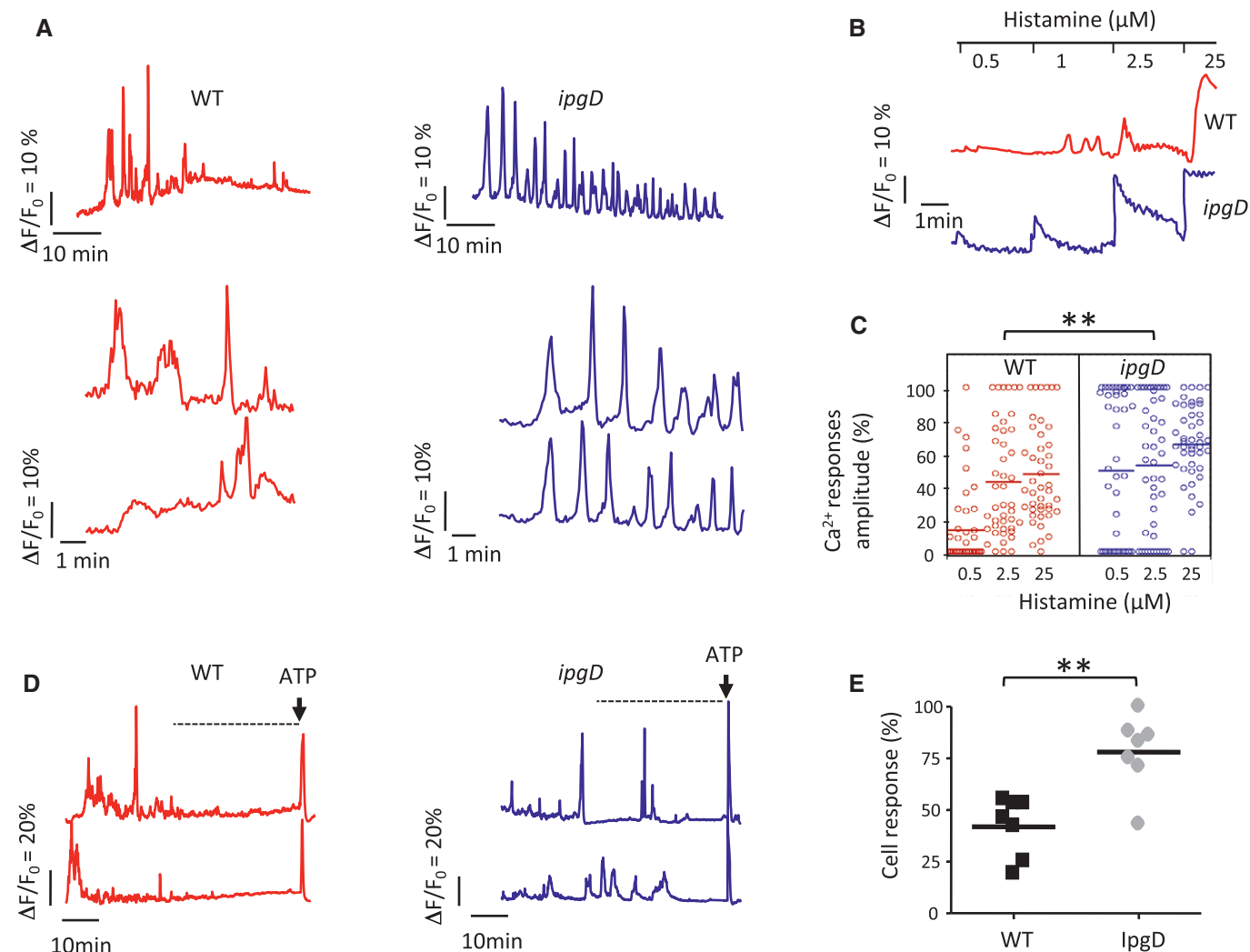


Figure 5. IpgD shapes global Ca^{2+} responses and inhibits InsP_3 -mediated signaling during prolonged infection kinetics.

Cells were loaded with the Ca^{2+} indicators Fura-2-AM (A–C) or Fluo-4-AM (D, E) and challenged with WT *Shigella* (red) or the *ipgD* mutant (blue). Samples were subjected to Ca^{2+} imaging (Materials and Methods). Changes in the ratio of Fura-2 fluorescence intensity (ΔR) were calculated relative to the resting ratio value (R_0) as $\Delta R/R_0$.

A Representative traces of single cell global Ca^{2+} responses are shown for challenge with the indicated strains.

B Representative traces of infected HeLa cells stimulated with histamine at the indicated concentrations at 90 min post-infection.

C Amplitude of Ca^{2+} responses relative to the maximal response upon stimulation at the indicated histamine concentrations of cells infected with the indicated bacteria for 90 min. Wilcoxon test, $**P < 0.01$.

D Representative traces of global Ca^{2+} responses are shown for polarized TC7 cells. The arrow indicates stimulation with 30 μM ATP.

E Dot plot representing the % of polarized TC7 cells challenged with the indicated bacterial strain, showing global Ca^{2+} responses during a 30-min period, 30 min following infection, and prior to ATP stimulation (dotted line in panel D) ($N = 7$, > 200 cells). Wilcoxon test: $**P = 0.007$.

Together, these results indicate that IpgD down-regulates InsP_3 -dependent Ca^{2+} responses during *Shigella* infection.

IpgD delays Ca^{2+} -dependent focal adhesion disappearance

Ca^{2+} is implicated in the majority of fundamental cell processes, including actin cytoskeletal reorganization or cell death induced during *Shigella* invasion of epithelial cells (Berridge *et al.*, 2000; Carneiro *et al.*, 2009; Bergounioux *et al.*, 2012). IpgD-mediated effects on Ca^{2+} signals are likely prominent early during infection, because InsP_3 levels were undetectable 2 h post-infection (Fig 1) and since at prolonged infection kinetics, plasma

membrane permeabilization leads to Ca^{2+} overload (Carneiro *et al.*, 2009; Tattoli *et al.*, 2012). Consistently, Ca^{2+} -dependent degradation of caspases 3 and 9 could be detected at 4 and 6 h post-infection, but only minor differences could be observed between cells challenged with *Shigella* WT or *ipgD* mutant strains (Appendix Fig S3). Also, as reported, IpgD stimulated the PI3K/Akt pathway and phosphorylation of the pro-apoptotic protein BAD (Pendaries *et al.*, 2006; Ramel *et al.*, 2011), but little difference was observed when cells were challenged in the absence of Ca^{2+} (Appendix Fig S3).

Remarkably, however, at 2 h post-infection, the *ipgD* mutant was 2.8-fold more cytotoxic compared to WT *Shigella* (Fig 6A),

an effect that was not observed in the absence of extracellular Ca^{2+} (Fig 6B). As expected from the InsP_3 kinetics, this difference in cytotoxicity did not evolve during further bacterial incubation (Fig 6A). The “hyper-cytotoxicity” associated with the *ipgD* mutant was accompanied by a Ca^{2+} -dependent cell retraction, suggesting that it resulted from cell detachment (Fig EV5A and B). We thus tested the effects of IpgD on cell adhesion structures. As shown in Fig 6C, cells infected with WT *Shigella* showed pronounced peripheral and radially oriented talin-containing focal adhesions (FAs), similar to uninfected cells or cells infected with the T3SS-deficient *mxiD* strain (Figs 6C and EV5). In contrast, cells infected with the *ipgD* mutant showed fewer FAs as early as an hour post-infection, with an average number of 13.2 ± 2.0 (SEM) FAs/cell compared to 21.4 ± 1.2 (SEM) FAs/cell for WT-

infected cells, in association with a decrease in the cell adhesion surface (Fig 6D and E). In addition, the percentage of cells showing FA disappearance was lower in cells infected with WT *Shigella* compared to *ipgD* mutant with kinetics that inversely mirrored that of cells showing large FAs (Fig EV5C) and paralleled that observed for cytotoxicity (Fig 6A). Quantification of anti-LPS immunofluorescence as a proxy indicated that the decrease in FAs was not due to a difference in bacterial load (Fig EV5E).

In polarized TC7 cells, bacteria were detected apically following a 90-min incubation period, several microns above the cell basal side where FAs were detected (Appendix Fig S4A). A reduction in FAs was observed for cells infected with wild-type *Shigella* compared to control non-infected cells (Appendix Fig S4). As

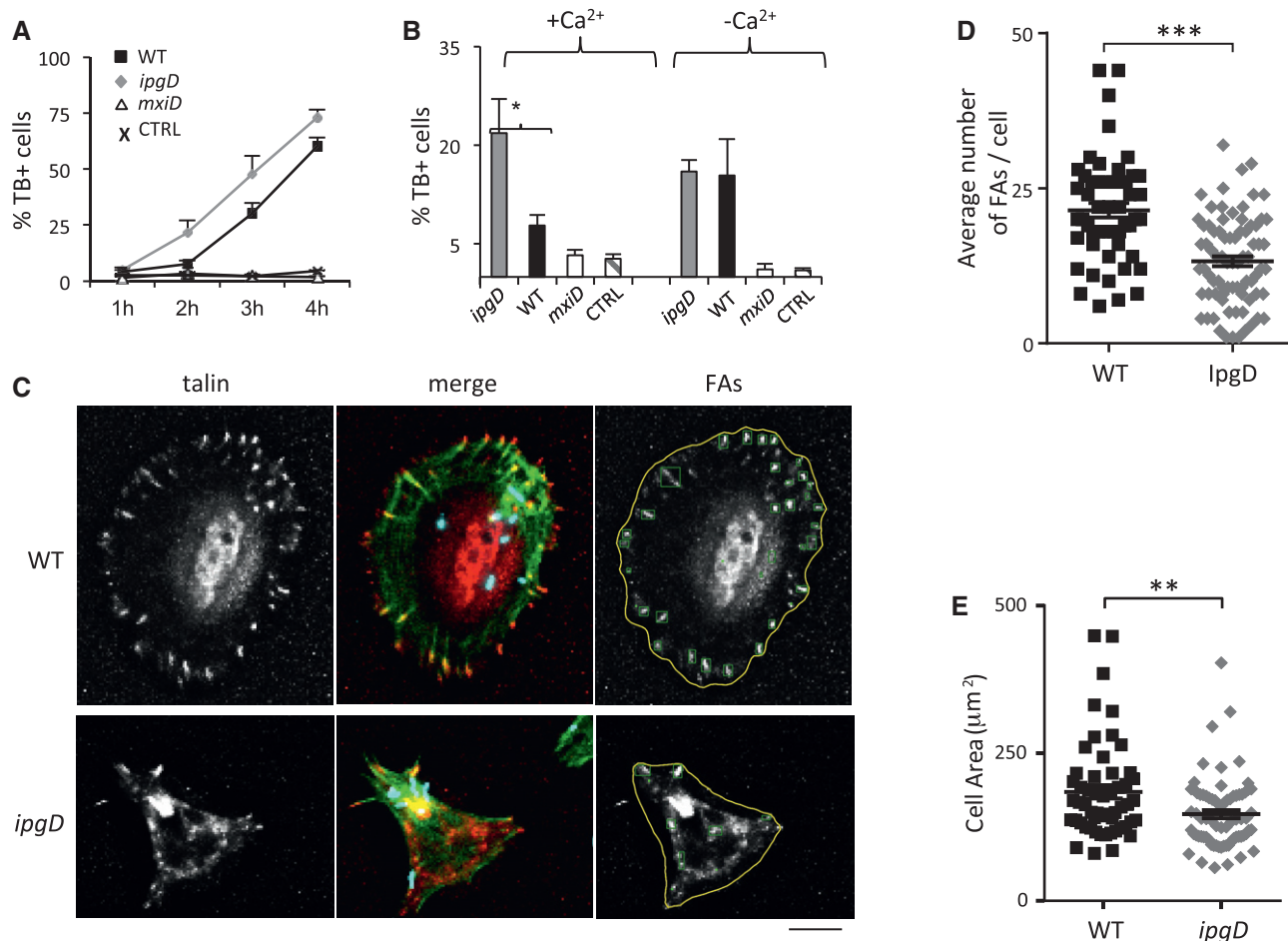


Figure 6. IpgD prevents Ca^{2+} -dependent early cytotoxicity linked to cell detachment induced by *Shigella*.

- A** Cells were challenged with wild-type *Shigella* (black squares) or the *ipgD* mutant (gray diamonds) for the indicated time points, and non-viable cells were scored by trypan blue staining. Representative experiments performed with triplicate determinations, $n > 1,000$ cells per point. The results are expressed as the average percentage of trypan blue-positive cells \pm SEM.
- B** Average percentage of trypan blue-positive cells \pm SEM following bacterial challenge with the indicated strains for 2 h in the absence (- Ca^{2+}) or presence (+ Ca^{2+}) of extracellular Ca^{2+} . CTRL: non-infected cells. $N = 3$, > 30 cells. Unpaired t-test, $*P = 0.0283$.
- C** Talin-GFP-transfected cells were challenged with the indicated *Shigella* strains for 1 h and processed for immunofluorescence staining. Talin: representative projection of deconvolved epifluorescence microscopy planes showing cells challenged with the indicated *Shigella* strains. Merge: actin: red, talin: green; bacteria: blue. FAs: detection of FAs performed using an automated algorithm (Materials and Methods). Scale bar, 5 μm .
- D** The average number of FAs/cell \pm SEM was determined for cells infected with the indicated bacteria as in (C). $N = 3$, > 30 cells. Unpaired t-test, $***P \leq 0.001$.
- E** The average cell area \pm SEM was determined for cells infected with the indicated bacteria as in (C). $N = 3$, > 30 cells. Wilcoxon test, $**P = 0.0031$.

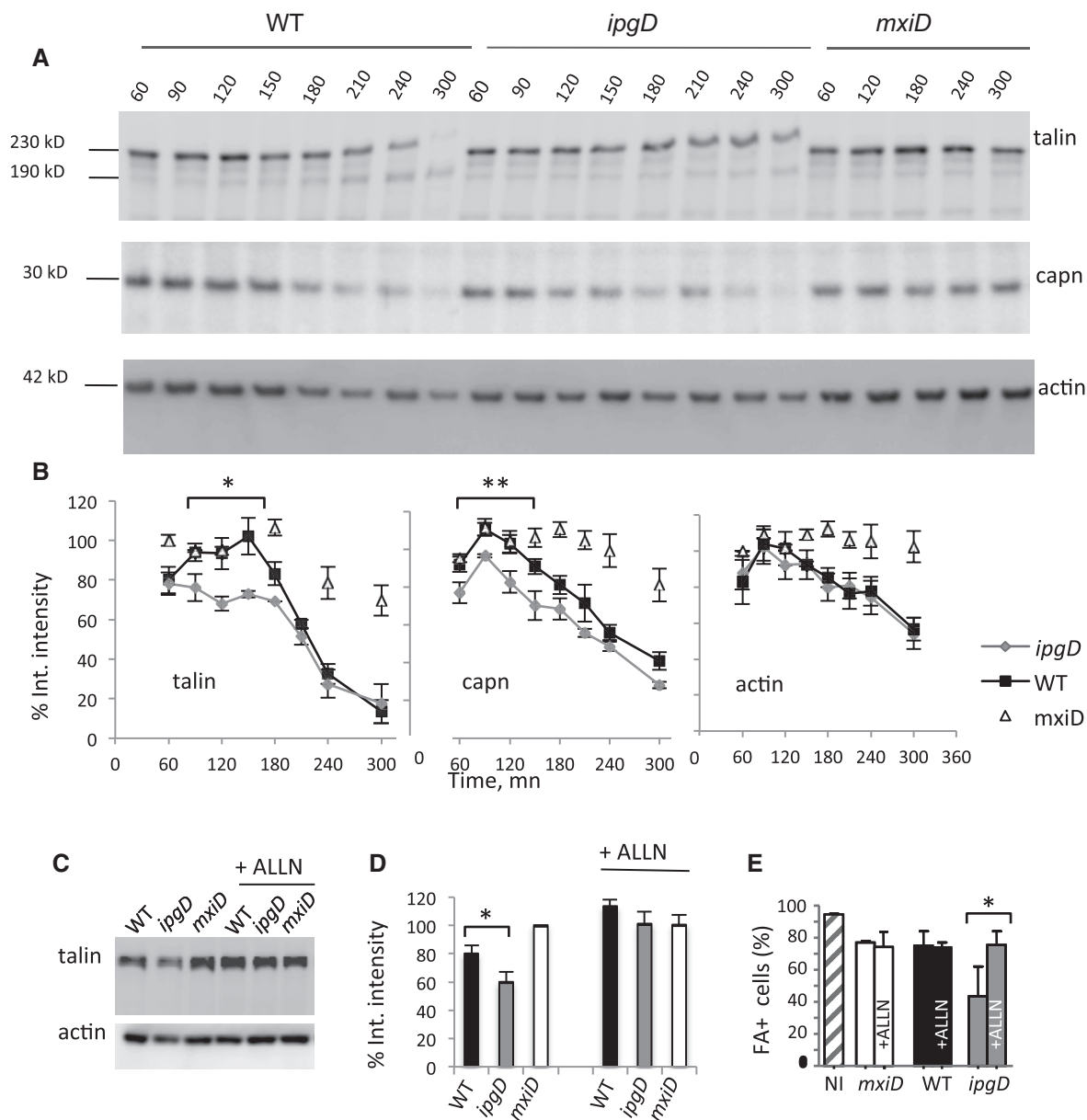


Figure 7. IpgD delays Ca^{2+} -dependent calpain activation and talin cleavage during *Shigella* invasion.

A Cells were infected with bacterial strains for the time indicated in minutes. Infected-cell lysates were analyzed by Western blotting using antibodies directed against the indicated proteins. A representative experiment is shown. Migration of the molecular weight markers is indicated.

B The average integrated intensity of bands \pm SEM corresponding to the indicated proteins was determined from at least three independent experiments and expressed as a percentage of that determined for control cells challenged with the non-invasive *mxiD* mutant. Cells were infected for the indicated incubation time with wild-type *Shigella* (black squares), the *ipgD* mutant (gray diamonds), or the *mxiD* mutant (empty triangles) strains. Statistical tests performed for values between 90 and 180 min. ANCOVA test, * $P = 0.01122$. ** $P = 0.008$.

C Cells were pre-treated with the calpain inhibitor ALLN at a final concentration of 10 μM for 1 h and challenged with bacteria for 1 h. Cell lysates were analyzed by anti-talin or anti-actin Western blotting. A representative experiment is shown.

D The average integrated intensity \pm SEM of the talin band was determined in independent experiments for the indicated bacterial strain. $N = 3$, Wilcoxon test, * $P < 0.05$.

E The relative percentage of cells challenged with the indicated strains and presenting large FAs \pm SEM is shown. $n > 30$ cells, $N = 2$. Wilcoxon test, * $P < 0.05$.

Source data are available online for this figure.

observed for HeLa cells, however, the decrease in FAs was significantly more pronounced in cells challenged with the *ipgD* mutant, or the *ipgD* mutant complemented with catalytically inactive IpgD C438S relative to wild-type *Shigella* (Appendix Fig S4B). As

expected, complementation of the *ipgD* mutant with wild-type IpgD led to a less severe reduction in FAs (Appendix Fig S4B).

Together, these results indicate that IpgD delays FA disassembly during *Shigella* infection of epithelial cells.

IpgD regulates the Ca^{2+} -dependent activation of calpain and talin cleavage

The physiological disassembly of focal adhesions is triggered by cleavage of talin by the Ca^{2+} -dependent protease calpain and depends on InsP_3 -mediated Ca^{2+} oscillations (Franco *et al*, 2004; Sorimachi & Ono, 2012). As previously described, cell infection with WT *Shigella* led to calpain activation that was detected starting from 3 h post-infection as assessed by the autoproteolytic cleavage of the small regulatory subunit Capn4 (Fig 7A and B) (Bergounioux & Arbibe, 2012; Sorimachi *et al*, 2012). Consistent with the kinetics of talin cleavage and as opposed to WT *Shigella*, the *ipgD* mutant induced calpain activation at the onset of bacterial challenge (Fig 7A and B). As expected, calpain activation depended on the presence of Ca^{2+} and was not observed with the *mxiD* mutant (Fig 7A and B, and Appendix Fig S5). Cell treatment with the calpain inhibitor ALLN prevented the degradation of talin induced by WT *Shigella* or the *ipgD* mutant strain, indicating the key role of calpain in the disassembly of focal adhesions (Fig 7C and D, and Appendix Fig S6).

These results indicate that IpgD delays the Ca^{2+} -dependent activation of calpain, talin cleavage, and focal adhesion disassembly, during cell infection by *Shigella*.

Discussion

In this report, we provide evidence for a key role of IpgD in regulating local and global Ca^{2+} signals during *Shigella* infection of epithelial cells. We show that IpgD plays a major role in the confinement of Ca^{2+} responses at invasion sites. In its absence, *Shigella* induces sharp and oscillating global Ca^{2+} responses, due to higher InsP_3 levels during bacterial invasion. Through modeling studies, we provide a mechanistic explanation for the IpgD-mediated confinement of Ca^{2+} responses at invasion sites, based on the observed increased InsP_3 levels and higher diffusion rates. Because of the non-linear relationship between InsP_3 and Ca^{2+} , modest variations in InsP_3 concentration can indeed induce drastic differences in Ca^{2+} release from the ER at invasion sites (Dupont *et al*, 2011; Tran Van Nhieu *et al*, 2013). This effect is further amplified by the increased recruitment of InsP_3 receptors observed at invasion sites induced by the *ipgD* mutant. How precisely IpgD regulates InsP_3 receptors recruitment is not clear and probably pertains to the general and long-standing debate over InsP_3 receptor clustering upon agonist stimulation. The observation that increased InsP_3 receptor recruitment at *Shigella* invasion sites correlates with higher InsP_3 levels induced by the *ipgD* mutant is in line with works showing oligomerization of InsP_3 receptors upon InsP_3 binding (Tateishi *et al*, 2005; Taufiq Ur *et al*, 2009). According to this view, increased InsP_3 levels would favor the oligomerization and entrapping of InsP_3 receptors by diffusion–capture in a process likely favored by the meshwork of polymerized actin at *Shigella* invasion sites (Tran Van Nhieu *et al*, 2013).

Considering the differential patterns of Ca^{2+} responses between WT *Shigella* and the *ipgD* mutant, the occurrence and duration of responses are likely the predominant parameters accounting for the IpgD-mediated regulation of calpain activity during the early stages of infection. According to this view, IpgD prevents calpain

activation during cell infection by limiting the number and duration of responses during the early stages of bacterial infection. Cell death comes as an ineluctable fate associated with *Shigella* intracellular replication and the permeabilization of the plasma membranes. *Shigella*, however, expresses various type III effectors to delay cell death or detachment. OspC3 prevents rapid apoptotic death (Kobayashi *et al*, 2013). Interestingly, apoptotic death induced by the *ospC3* mutant is not accompanied by the usually observed loss

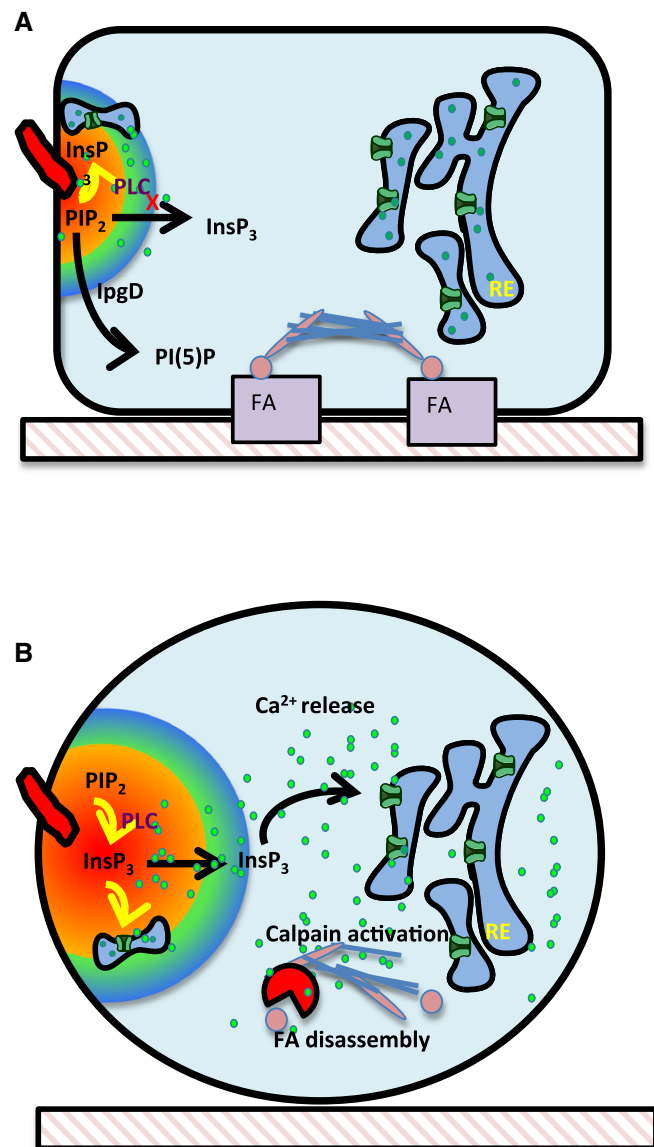


Figure 8. Model for IpgD-mediated regulation of Ca^{2+} signals and FA disassembly during *Shigella* invasion of epithelial cells.

- A** IpgD hydrolyzes PI(4,5)P₂ thereby limiting the substrate pool available to PLCs at bacterial invasion sites. This results in a decrease in InsP_3 production which, combined with restricted diffusion, favors long-lasting local Ca^{2+} responses at *Shigella*-induced actin foci.
- B** In the absence of IpgD, bacterial-induced actin foci are less restrictive in diffusion, and increased InsP_3 levels stimulate Ca^{2+} release. Increased cytosolic Ca^{2+} activates the calpain-dependent cleavage of talin and focal adhesion disassembly.

of cell adhesion (Kobayashi *et al*, 2013). By targeting ILK (integrin-linked kinase), OspE was shown to reinforce adhesions (Kim *et al*, 2009). We show here that IpgD contributes to delay such cell detachment by preventing the Ca^{2+} -dependent calpain activation and cleavage of talin (Fig 8). The VirA type III effector was proposed to induce early calpain activation through calpastatin degradation in a Ca^{2+} -dependent manner during *Shigella* invasion (Bergounioux & Arbibe, 2012). We show here that by preventing InsP_3 -mediated Ca^{2+} release, IpgD inhibits the early activation of calpain, but does not prevent the Ca^{2+} -dependent activation of calpain at late stages of infection. Thus, through its effects on Ca^{2+} signaling, IpgD regulates the function of various type III effectors during *Shigella* invasion of epithelial cells.

Because of the versatility of Ca^{2+} signaling, the effects of IpgD on the regulation of Ca^{2+} signals are likely to impact various processes during *Shigella* infection. Ca^{2+} regulates the activity of kinases and phosphatases, and their relative catalytic on/off constants for Ca^{2+} are generally recognized as main components of the decoding of Ca^{2+} signals (Smedler & Uhlen, 2014). Specifically, the persistent duration of RATPs induced by WT *Shigella* will be decoded differently than the repeated Ca^{2+} spikes induced in the absence of IpgD. Such differential Ca^{2+} decoding could impact on the reported IpgD functions in impairment of lymphocyte migration or recruitment of exocytic vesicles during vacuolar rupture following *Shigella* invasion (Konradt *et al*, 2011; Mellouk *et al*, 2014).

Materials and Methods

Bacterial strains, cell line, and reagents

The invasive *Shigella flexneri* 5a wild-type stain (M90T), the non-invasive *mxlD* mutant, and the *ipgD* mutant expressing the AfaE afimbrial adhesin of uropathogenic *E. coli* were described previously (Tran Van Nhieu *et al*, 2003). Bacteria were grown at 37°C in trypticase soy broth. HeLa cells were from ATCC and grown in RPMI + Glutamax medium (RPMI1640; GIBCO, Invitrogen) supplemented with 5% fetal calf serum (FCS) and grown at 37°C with 5% CO_2 . Caco-2/TC7 cells were described previously (Chantret *et al*, 1994) and were grown in DMEM + Glutamax medium (Dulbecco's modified Eagle's medium; GIBCO, Invitrogen) containing 4.5 g/l glucose, supplemented with 10% FCS and non-essential amino acids. The rabbit polyclonal antibody against the type1 InsP_3 receptor was from ABR Affinity BioReagents. The monoclonal antibody against the type 3 InsP_3 receptor was from Thermo Fisher. The anti-*Shigella* LPS FlexV polyclonal antibody was described previously (Mounier *et al*, 2009). The mouse monoclonal anti-capn4 antibody and anti-talin clone 8D4 antibodies were from Biovision and Sigma Corporation, respectively. The phalloidin-A488, phalloidin-A633, and anti-rabbit IgG-Alexa547 were from Thermo Fisher Scientific. The fluorescent probes calcein-AM and Fluo-4-AM were from Invitrogen. The PLC inhibitor U73122 and the calpain inhibitor ALLN were from Sigma Corporation. [^3H] myo-inositol (15.0 Ci/mmol) was from Amersham. [^3H] $\text{Ins}(1,4,5)\text{P}_3$ (21.4 Ci/mmol), [^3H] $\text{Ins}(1,3,4,5)\text{P}_4$ (21.0 Ci/mmol), and [^3H] IP_6 (21.4 Ci/mmol) used as standards to calibrate the HPLC SAX column were from Perkin-Elmer.

Plasmid constructions

The plasmid constructs expressing the GFP-PH-PLC $_{\delta 1}$ and GFP-talin were described previously (Franco *et al*, 2004; Balla & Varnai, 2009).

Bacterial infection

For immunofluorescence staining experiments, HeLa cells were plated the day before onto coverslips in 6-well plates at a density of 1×10^5 cells/well. When mentioned, cells were transfected using the JetPei TM reagent (Polyplus) according to the manufacturer's instructions. TC7 cells were plated onto coverslips in 6-well plates at a density of 4×10^5 cells/well and allowed to polarize for 7 days, with a daily change of medium upon cell confluency. Bacterial strains grown to exponential phase were resuspended in RPMI1640 medium or DMEM for challenge of HeLa cells and TC7 cells, respectively, supplemented with 50 mM HEPES pH 7.5. Cells were challenged with bacteria at a MOI of 40 and 80, for challenge of HeLa cells and TC7 cells, respectively, for 15 min at 21°C prior to incubation at 37°C for the indicated period. At the indicated time points, cells were washed three times, fixed with 3.7% paraformaldehyde (PFA) for 20 min at 21°C, and with ethanol:acetone 1:1 for 5 min at 21°C, and processed for immunofluorescence staining of $\text{InsP}_3\text{R1}$ and $\text{InsP}_3\text{R3}$ or talin, respectively.

Inositol-polyphosphate measurements

HeLa cells were labeled with 100 $\mu\text{Ci/ml}$ [^3H] myo-inositol for 3 days, and the levels of inositol-polyphosphates were measured as described previously (Leyman *et al*, 2007).

Immunofluorescence microscopy analysis

After fixation with PFA, cells were permeabilized with 0.1% Triton X-100 for 4 min. Samples were washed three times with PBS and blocked with PBS containing 5% FCS for 20 min. Cells were incubated for 1 h with primary antibodies at the following dilution: rabbit polyclonal anti-type 1 InsP_3 receptor antibody (1:2,000), mouse monoclonal anti-type 3 InsP_3 receptor antibody (1:200), mouse monoclonal anti-talin (1:300), and rabbit polyclonal anti-FlexV LPS antibody (1:5,000); and incubated with the corresponding secondary anti-rabbit IgG or anti-mouse IgG antibodies, or Alexa-conjugated phalloidin at a dilution of 1:200. Samples were mounted in Dako mounting medium (DAKO) and analyzed using an Eclipse Ti microscope (Nikon) equipped with a 100 \times objective, a CSU-X1 spinning disk confocal head (Yokogawa), and a Coolsnap HQ2 camera (Roper Scientific Instruments), controlled by the Metamorph 7.7 software. Analysis by epifluorescence microscopy was performed using a DMRIbe microscope (LEICA Microsystems) using 380-nm, 470-nm, or 546-nm LED source excitation, equipped with a Cascade 512 camera (Roper Scientific) driven by the Metamorph (7.7) software. Images were analyzed using the Metamorph software.

Image analysis

For the quantification of $\text{PI}(4,5)\text{P}_2$ enrichment fold, the average fluorescence intensity of the PH-PLC $_{\delta 1}$ probe of *Shigella* invasion foci in transfected cells corrected to background was normalized by the average fluorescence intensity of a control area in the same

transfected cell. A similar method was applied to quantify the enrichment fold of $\text{InsP}_3\text{R1}$ except that samples were subjected to quantitative immunofluorescence staining as described previously (Tran Van Nhieu *et al.*, 2013). For focal adhesion numbers and cell adhesion surface quantification, a semi-automated protocol was developed using Icy bioimaging software (de Chaumont *et al.*, 2012). Briefly, epifluorescent microscopy planes spaced by 0.2 μm were deconvolved with the Meinel algorithm using the Metamorph (7.7) software and measured PSFs. Large talin-containing structures were detected using the inbuilt “Wavelet Spot Detector” plugin on the maximum Z-projections of deconvolved GFP-talin fluorescent planes. The identified structures were overlaid in a binary mask obtained from thresholded projections of F-actin labeled images, using the “Moments method”. Focal adhesions were detected as structures positive for talin and actin. Cell area was identified using the inbuilt Active Contours Icy plugin in the GFP-talin channel.

Calcium imaging

HeLa cells seeded on coverslips were loaded with 3 μM Fluo-4-AM in EM buffer containing 120 mM NaCl, 7 mM KCl, 1.8 mM CaCl_2 , 0.8 mM MgCl_2 , 5 mM glucose, and 25 mM HEPES (pH = 7.3) for 30 min at 21°C, washed in EM buffer, and further incubated for 20 min. For TC7 cells, pluronate was added during the Fluo-4-AM loading procedure at a final concentration of 0.1%. Samples were analyzed at 33°C on an inverted Leica DMRBe fluorescence microscope, equipped with light-emitting diode 470-nm illuminating sources and a 480-nm band-pass excitation filter, a 505-nm dichroic filter, and a 527-nm band-pass emission filter driven by the Metamorph software from Roper Scientific Instruments. For analysis of local Ca^{2+} variations, images were captured using a Cascade 512B EM-CCD back-illuminated camera in a stream mode, with an acquisition every 30 ms. Changes in the ratio of Fura-2 (ΔR) or Fluo-4 fluorescence intensity (ΔF) were calculated relative to the resting ratio or fluorescence value (R_0 or F_0) as $\Delta R/R_0$ or $\Delta F/F_0$, respectively. Cells showing local Ca^{2+} responses were scored by high-speed fluorescence microscopy (HSFM). The average percentage of responsive cells showing a detectable Ca^{2+} response during the length of the analysis was determined.

FRAP analysis

Cells were cultured on 25-mm-diameter coverslips (Marienfeld) and loaded with 3 μM calcein-AM (3 kDa) in EM buffer for 30 min. Cells were mounted in an observed chamber on a plate of an inverted spinning disk confocal microscopy heated at 37°C (Nikon Eclipse Ti) and analyzed with a 60 \times objective, using an EM-CCD camera equipped with a FRAP module and driven by the Metamorph software (Roper Scientific Instruments), allowing to the acquisition of images during the bleaching phase. Samples were infected with *ipgD* mutant or WT for 10 min; then, *Shigella*-induced foci were subjected to FRAP (fluorescence recovery after photobleaching) analysis, essentially as described previously (Tran Van Nhieu *et al.*, 2013). Fluorescence recovery curves corresponding to the normalized intensity in the bleached area were performed; average from several measurements showed good-quality fit with a single component diffusion (> 30 foci, $N = 4$).

Modeling of intracellular Ca^{2+} and InsP_3 dynamics during bacterial invasion

As an improvement to our previous model, we took into account the possible effects of molecular noise, because of the random character of *Shigella*-induced Ca^{2+} responses and the well-established stochastic nature of Ca^{2+} dynamics. Using the Gillespie’s algorithm, we developed a stochastic version of the model used in our previous analysis to investigate the origin of the Ca^{2+} responses confined at the invasion site during *Shigella* invasion (Tran Van Nhieu *et al.*, 2013). This model consists in three differential equations describing the evolution of the fraction of inhibited InsP_3 receptors (R_i), the concentration of cytosolic Ca^{2+} (C), and the concentration of InsP_3 (I):

$$\frac{dR_i}{dt} = k_+(1 - R_i) \frac{C^{n_i}}{1 + \left(\frac{C}{K_A}\right)^{n_A}} - k_- R_i \quad (1)$$

$$\frac{\partial C}{\partial t} = \alpha k_1(\bar{r}) \cdot (b + R_a) - V_p \frac{C^2}{K_p^2 + C^2} + D_C(\bar{r}) \nabla^2 C \quad (2)$$

$$\frac{\partial I}{\partial t} = V_b + J_{IP}(\bar{r}) - k_d I + D_I(\bar{r}) \nabla^2 I \quad (3)$$

where $R_a = (1 - R_i) \frac{1}{K_A + I} \frac{C^{n_A}}{K_A^{n_A} + C^{n_A}}$ represents the fraction of open (active) receptors.

Equations are described in Tran Van Nhieu *et al.* (2013). Parameters are defined in Table EV1, where their values in the simulations are also provided. Initial conditions correspond to the steady-state situation in the absence of bacterial invasion. A typical HeLa cell is simulated as a two-dimensional $26 \times 10 \mu\text{m}$ system, in which the *Shigella* actin focus is defined by its lower diffusivity, higher density of InsP_3 receptors, and higher rate of InsP_3 synthesis and covers the $6 \times 6 \mu\text{m}$ top central region (Appendix Fig S7). In most simulations, this system is discretized into 13×5 mesh points; results were not qualitatively affected when dividing by 2 the size of the grid.

Fluctuations due to molecular noise are taken into account using the Gillespie’s algorithm (Gillespie, 1976). This method associates a probability to each kinetic transition considered in the model. At each grid point, diffusion is treated as a kinetic reaction by computing the probability that an InsP_3 molecule or a Ca^{2+} ion will “jump” to a nearest-neighbor grid point. This probability depends on the deterministic diffusion coefficient and on the difference between the number of molecules at the considered grid point and at each of its neighbor (Kraus *et al.*, 1996). At each time step of the simulation, the algorithm stochastically determines the change that takes place corresponding to a reactive or diffusive step, according to its relative propensity related to the number of molecules involved in the reaction and on the rate constants. The level of molecular noise, which determines the amplitude of the fluctuations around the corresponding deterministic evolution, is scaled by parameter Ω . The higher the Ω , the larger the number of molecules considered in the simulations and the lower the amplitude of the fluctuations. Here, two different Ω are considered, to take into account that the number of InsP_3 and Ca^{2+} molecules/ions is not scaled by the same factor than the number of InsP_3 receptors (Dupont *et al.*, 2008). In the simulations presented in Fig 4, $\Omega_1 = 10^5$ for InsP_3 and Ca^{2+} , and $\Omega_2 = 6,000$ for the InsP_3 receptors. The scoring of local and global responses during infection with WT *Shigella*, the *ipgD* mutant, or

the theoretical scenario of infection with WT *Shigella* in the presence of the high InsP_3 levels observed for the *ipgD* mutant was performed on at least 25 determinations for each sample. Concentrations shown in ordinate correspond to the number of particles divided by the corresponding Ω_i .

Trypan blue exclusion test

To quantify cell death, following bacterial infection, samples' supernatants were recovered and cells were pelleted by centrifugation for 5 min at $800 \times g$. Following resuspension, these cells were stained with PBS containing 0.4% trypan blue for 5 min. Adherent cells were also trypsinized and subjected to trypan blue staining. Cells were scored using a Malassez chamber using bright-field microscopy and a $20\times$ objective. The ratio of dead cells was as $(S_b + A_b / S_t + A_t) \times 100$, where S_b and A_b represent the number of trypan blue-positive cells in the supernatant and attached cells, respectively, and the S_t and A_t represent for the total number of cells in the supernatant and attached cells, respectively. For each determination, the results shown are representative of over 2,000 cells scored in at least three independent experiments. For experiments without extracellular Ca^{2+} , EGTA was added to the RPMI medium at a final concentration of 2 mM, a concentration that was determined to suppress a detectable increase in the fluorescence of Fluo-4-AM-loaded cells following ionophore challenge.

Western blotting

Cells challenged with *Shigella* strains were scraped in 200 μl Laemmli sample lysis buffer. Western blot analysis was performed using the following primary and secondary antibody dilutions: anti-calpn4 (1:50,000); anti-talin (1:10,000); anti-actin (1:50,000); anti-mouse IgG (1:20,000); and anti-rabbit IgG (1:10,000) coupled to peroxidase. Immunoreactive bands were detected by chemiluminescence using the ECL plus reagent (GE Healthcare Biosciences) and the FujiFilm LAS 4000 system.

Statistical analysis

Statistical analysis was performed using Student's *t*-test, Wilcoxon rank-sum test, or one-way analysis of variance (ANOVA). The error bars represent the standard error of the mean. *P*-value < 0.05 was considered significant different between two groups, indicated by asterisks: $*P \leq 0.05$; $**P \leq 0.01$; and $***P \leq 0.001$.

Expanded View for this article is available online.

Acknowledgements

The work was supported by the ANR grants MITOPATHO and PATHIMMUN, grant from Tournesol program No. 31268YG, and grants from the Labex Memo-life and PSL IDEX Shigaforce. CHS is a recipient of a PhD grant from the China Scholarship Council. DA is a recipient of a CONACYT grant and Labex Memolife. CV-G was a recipient of the PSL IDEX grant. NC is a recipient of a Marie-Curie IRG grant. BW and GD are Research Fellow and Research Director at the Belgian F.R.S.-F.N.R.S., respectively. This work was supported by the Fonds de la Recherche Scientifique-FNRS under Grant No. J0043.14 and by the Fonds David and Alice Van Buuren. JE was supported by an ERC Starting ("Ruptef-fects" No. 261166) and a Consolidator Grant ("Endosubvert" No. 682809). LC,

GD, and GTVN are recipients of a WBI-France Exchange Program (Wallonie-Bruxelles International, Fonds de la Recherche Scientifique, Ministère Français des Affaires étrangères et européennes, Ministère de l'Enseignement supérieur et de la Recherche dans le cadre des Partenariats Hubert Curien).

Author contributions

CHS planned and performed most of the experimentation. GD and BW did the Ca^{2+} responses simulations and models. DIA analyzed the data and performed the statistical analysis. CE, NC, KD, SB, CS, and AL provided with key technical help. JE and LA provided with materials. CE and PS planned experiments and discussed the results. CV-G performed statistical analysis. LC and GTVN planned, performed, and analyzed experiments. GD, BW, LC, and GTVN wrote the manuscript.

Conflict of interest

The authors declare that they have no conflict of interest.

References

- Ashida H, Ogawa M, Kim M, Mimuro H, Sasakawa C (2012) Bacteria and host interactions in the gut epithelial barrier. *Nat Chem Biol* 8: 36–45
- Ashida H, Kim M, Sasakawa C (2014) Manipulation of the host cell death pathway by *Shigella*. *Cell Microbiol* 16: 1757–1766
- Ashida H, Mimuro H, Sasakawa C (2015) *Shigella* manipulates host immune responses by delivering effector proteins with specific roles. *Front Immunol* 6: 219
- Balla T, Varnai P (2009) Visualization of cellular phosphoinositide pools with GFP-fused protein-domains. *Curr Protoc Cell Biol* 42: 24.4.1–24.4.27
- Bergounioux J, Arbibe L (2012) Calpain activation by *Shigella flexneri* regulates key steps in the life and death of bacterium's epithelial niche. *Med Sci (Paris)* 28: 1029–1031
- Bergounioux J, Elisee R, Prunier AL, Donnadiou F, Sperandio B, Sansonetti P, Arbibe L (2012) Calpain activation by the *Shigella flexneri* effector VirA regulates key steps in the formation and life of the bacterium's epithelial niche. *Cell Host Microbe* 11: 240–252
- Berridge MJ, Lipp P, Bootman MD (2000) The versatility and universality of calcium signalling. *Nat Rev Mol Cell Biol* 1: 11–21
- Boal F, Puhar A, Xuereb JM, Kunduzova O, Sansonetti PJ, Payraastre B, Tronchere H (2016) PISP triggers ICAM-1 degradation in shigella infected cells, thus dampening immune cell recruitment. *Cell Rep* 14: 750–759
- Carneiro LA, Travassos LH, Soares F, Tattoli I, Magalhaes JG, Bozza MT, Plotkowski MC, Sansonetti PJ, Molkentin JD, Philpott DJ, Girardin SE (2009) *Shigella* induces mitochondrial dysfunction and cell death in nonmyeloid cells. *Cell Host Microbe* 5: 123–136
- Chantret I, Rodolose A, Barbat A, Dussaulx E, Brot-Laroche E, Zweibaum A, Rousset M (1994) Differential expression of sucrase-isomaltase in clones isolated from early and late passages of the cell line Caco-2: evidence for glucose-dependent negative regulation. *J Cell Sci* 107(Pt. 1): 213–225
- de Chaumont F, Dallongeville S, Chenouard N, Herve N, Pop S, Provoost T, Meas-Yedid V, Pankajakshan P, Lecomte T, Le Montagner Y, Lagache T, Dufour A, Olivo-Marin J-C (2012) Icy: an open bioimage informatics platform for extended reproducible research. *Nat Methods* 9: 690–696
- Dupont G, Abou-Lovergne A, Combettes L (2008) Stochastic aspects of oscillatory Ca^{2+} dynamics in hepatocytes. *Biophys J* 95: 2193–2202
- Dupont G, Lokenye EF, Challiss RA (2011) A model for Ca^{2+} oscillations stimulated by the type 5 metabotropic glutamate receptor: an unusual

- mechanism based on repetitive, reversible phosphorylation of the receptor. *Biochimie* 93: 2132–2138
- Franco SJ, Rodgers MA, Perrin BJ, Han J, Bennin DA, Critchley DR, Huttenlocher A (2004) Calpain-mediated proteolysis of talin regulates adhesion dynamics. *Nat Cell Biol* 6: 977–983
- Galan JE, Lara-Tejero M, Marlovits TC, Wagner S (2014) Bacterial type III secretion systems: specialized nanomachines for protein delivery into target cells. *Annu Rev Microbiol* 68: 415–438
- Gillespie DT (1976) General method for numerically simulating stochastic time evolution of coupled chemical-reactions. *J Comput Phys* 22: 403–434
- Kim M, Ogawa M, Fujita Y, Yoshikawa Y, Nagai T, Koyama T, Nagai S, Lange A, Fassler R, Sasakawa C (2009) Bacteria hijack integrin-linked kinase to stabilize focal adhesions and block cell detachment. *Nature* 459: 578–582
- Kobayashi T, Ogawa M, Sanada T, Mimuro H, Kim M, Ashida H, Akakura R, Yoshida M, Kawalec M, Reichhart JM, Mizushima T, Sasakawa C (2013) The *Shigella* OspC3 effector inhibits caspase-4, antagonizes inflammatory cell death, and promotes epithelial infection. *Cell Host Microbe* 13: 570–583
- Konradt C, Frigimelica E, Nothelfer K, Puhar A, Salgado-Pabon W, di Bartolo V, Scott-Algara D, Rodrigues CD, Sansonetti PJ, Phalipon A (2011) The *Shigella flexneri* type three secretion system effector IpgD inhibits T cell migration by manipulating host phosphoinositide metabolism. *Cell Host Microbe* 9: 263–272
- Kraus M, Wolf B, Wolf B (1996) Crosstalk between cellular morphology and calcium oscillation patterns. Insights from a stochastic computer model. *Cell Calcium* 19: 461–472
- Kuehl CJ, Dragoi AM, Talman A, Agaisse H (2015) Bacterial spread from cell to cell: beyond actin-based motility. *Trends Microbiol* 23: 558–566
- LaRock DL, Chaudhary A, Miller SI (2015) Salmonellae interactions with host processes. *Nat Rev Microbiol* 13: 191–205
- Leyman A, Pouillon V, Bostan A, Schurmans S, Erneux C, Pesesse X (2007) The absence of expression of the three isoenzymes of the inositol 1,4,5-trisphosphate 3-kinase does not prevent the formation of inositol pentakisphosphate and hexakisphosphate in mouse embryonic fibroblasts. *Cell Signal* 19: 1497–1504
- Mellouk N, Weiner A, Aulner N, Schmitt C, Elbaum M, Shorte SL, Danckaert A, Enninga J (2014) *Shigella* subverts the host recycling compartment to rupture its vacuole. *Cell Host Microbe* 16: 517–530
- Mounier J, Vasselon T, Hellio R, Lesourd M, Sansonetti PJ (1992) *Shigella flexneri* enters human colonic Caco-2 epithelial cells through the basolateral pole. *Infect Immun* 60: 237–248
- Mounier J, Popoff MR, Enninga J, Frame MC, Sansonetti PJ, Van Nhieu GT (2009) The IpaC carboxyterminal effector domain mediates Src-dependent actin polymerization during *Shigella* invasion of epithelial cells. *PLoS Pathog* 5: e1000271
- Muallem S (2005) Decoding Ca^{2+} signals: a question of timing. *J Cell Biol* 170: 173–175
- Murakami T, Ockinger J, Yu J, Byles V, McColl A, Hofer AM, Horng T (2012) Critical role for calcium mobilization in activation of the NLRP3 inflammasome. *Proc Natl Acad Sci USA* 109: 11282–11287
- Niebuhr K, Giurato S, Pedron T, Philpott DJ, Gaits F, Sable J, Sheetz MP, Parsot C, Sansonetti PJ, Payrastra B (2002) Conversion of PtdIns(4,5)P(2) into PtdIns(5)P by the *S. flexneri* effector IpgD reorganizes host cell morphology. *EMBO J* 21: 5069–5078
- Pendaries C, Tronchere H, Arbibe L, Mounier J, Gozani O, Cantley L, Fry MJ, Gaits-Iacovoni F, Sansonetti PJ, Payrastra B (2006) PtdIns5P activates the host cell PI3-kinase/Akt pathway during *Shigella flexneri* infection. *EMBO J* 25: 1024–1034
- Ramel D, Lagarrigue F, Pons V, Mounier J, Dupuis-Coronas S, Chicanne G, Sansonetti PJ, Gaits-Iacovoni F, Tronchere H, Payrastra B (2011) *Shigella flexneri* infection generates the lipid PIP5 to alter endocytosis and prevent termination of EGFR signaling. *Sci Signal* 4: ra61
- Rizzuto R, De Stefani D, Raffaello A, Mammucari C (2012) Mitochondria as sensors and regulators of calcium signalling. *Nat Rev Mol Cell Biol* 13: 566–578
- Romero S, Grompone G, Carayol N, Mounier J, Guadagnini S, Prevost MC, Sansonetti PJ, Van Nhieu GT (2011) ATP-mediated Erk1/2 activation stimulates bacterial capture by filopodia, which precedes *Shigella* invasion of epithelial cells. *Cell Host Microbe* 9: 508–519
- Shibao K, Fiedler MJ, Nagata J, Minagawa N, Hirata K, Nakayama Y, Iwakiri Y, Nathanson MH, Yamaguchi K (2010) The type III inositol 1,4,5-trisphosphate receptor is associated with aggressiveness of colorectal carcinoma. *Cell Calcium* 48: 315–323
- Smedler E, Uhlen P (2014) Frequency decoding of calcium oscillations. *Biochim Biophys Acta* 1840: 964–969
- Sorimachi H, Mamitsuka H, Ono Y (2012) Understanding the substrate specificity of conventional calpains. *Biol Chem* 393: 853–871
- Sorimachi H, Ono Y (2012) Regulation and physiological roles of the calpain system in muscular disorders. *Cardiovasc Res* 96: 11–22
- Strehler EE (2015) Plasma membrane calcium ATPases: from generic Ca^{2+} sump pumps to versatile systems for fine-tuning cellular Ca^{2+} . *Biochem Biophys Res Commun* 460: 26–33
- Tanner K, Brzovic P, Rohde JR (2015) The bacterial pathogen-ubiquitin interface: lessons learned from *Shigella*. *Cell Microbiol* 17: 35–44
- Tateishi Y, Hattori M, Nakayama T, Iwai M, Bannai H, Nakamura T, Michikawa T, Inoue T, Mikoshiba K (2005) Cluster formation of inositol 1,4,5-trisphosphate receptor requires its transition to open state. *J Biol Chem* 280: 6816–6822
- Tattoli I, Sorbara MT, Vuckovic D, Ling A, Soares F, Carneiro LA, Yang C, Emili A, Philpott DJ, Girardin SE (2012) Amino acid starvation induced by invasive bacterial pathogens triggers an innate host defense program. *Cell Host Microbe* 11: 563–575
- Taufiq Ur R, Skupin A, Falcke M, Taylor CW (2009) Clustering of InsP3 receptors by InsP3 retunes their regulation by InsP3 and Ca^{2+} . *Nature* 458: 655–659
- Thurley K, Tovey SC, Moenke G, Prince VL, Meena A, Thomas AP, Skupin A, Taylor CW, Falcke M (2014) Reliable encoding of stimulus intensities within random sequences of intracellular Ca^{2+} spikes. *Sci Signal* 7: ra59
- Tran Van Nhieu G, Clair C, Bruzzone R, Mesnil M, Sansonetti P, Combettes L (2003) Connexin-dependent inter-cellular communication increases invasion and dissemination of *Shigella* in epithelial cells. *Nat Cell Biol* 5: 720–726
- Tran Van Nhieu G, Kai Liu B, Zhang J, Pierre F, Prigent S, Sansonetti P, Erneux C, Kuk Kim J, Suh PG, Dupont G, Combettes L (2013) Actin-based confinement of calcium responses during *Shigella* invasion. *Nat Commun* 4: 1567
- Uhlen P, Fritz N (2010) Biochemistry of calcium oscillations. *Biochem Biophys Res Commun* 396: 28–32
- Valdivia R, Sedwick C (2014) Raphael Valdivia: how Chlamydia settles in. *J Cell Biol* 207: 4–5
- Weiner A, Mellouk N, Lopez-Montero N, Chang YY, Souque C, Schmitt C, Enninga J (2016) Macropinosomes are key players in early *shigella* invasion and vacuolar escape in epithelial cells. *PLoS Pathog* 12: e1005602